Krüppel-like factor **gene function in the ctenophore** ***Mnemiopsis*** **suggests an ancient role in promoting cell proliferation in metazoan stem cell niches**

Jason S Presnell[1,2], William E Browne[1,*]

[1]Department of Biology, University of Miami, Cox Science Center, 1301 Memorial Drive, Miami, FL 33146, USA

[2]Present Address: Department of Integrative Biology, Oregon State University, 3029 Cordley Hall, Corvallis, OR 97331, USA

*Correspondence: w.browne@miami.edu

Abstract

All animals possess pluripotent stem cells that during an organism's lifespan give rise to differentiated cell types and are capable of self-renewal. To date studies assessing the function of explicit genes driving the regulation of stem cell renewal and pluripotency have been characterized in bilaterians and a small number of cnidarians. Transcription factor genes critical for regulation of stem cell self-renewal and pluripotency include *Oct4*, *Sox2*, *Klf4, and c-myc* (OSKM) [1–3]. In particular, the role of *Klfs* in stem cell renewal and pluripotency has been thoroughly investigated [1,2,4–9]. In mouse embryonic stem cells the three *Krüppel-like factor* (*Klf*) genes *Klf2*, *Klf4*, and *Klf5* participate in an auto-regulatory activation loop and maintain a transcriptional circuit with *Oct4*, *Sox2*, *c-myc*, and *Nanog* regulating stem cell self-renewal [4]. While OSKM gene homologs have been found in the genomes of many metazoans [3,10,11], their function is unknown in non-bilaterians. Ctenophora, an ancient non-bilaterian lineage [12–14], possess putative stem cells [11,15,16] and have prodigious regenerative capacity [17,18], making them informative models for investigating the evolution and genetic underpinnings of stem cell maintenance in Metazoa. Ctenophores possess homologs of the OSKM genes [11,19–21], and while the expression patterns of ctenophore *Sox* paralogs are associated with high rates of cell proliferation in putative stem cell niches [11,19], little is known about *Pou*, *Klf*, or *c-myc* expression or function. Here we examine the expression of *Klf* homologs in the ctenophore *Mnemiopsis leidyi* and disrupt zygotic *Klf* gene function during embryogenesis using both morpholino oligonucleotides and CRISPR-Cas9. We find that zygotic *MleKlf5a* and *MleKlf5b* play a role in patterning the gastrovascular cavity, pharynx, apical organ, and tentacle bulbs in *M. leidyi*. Simultaneous zygotic knockdown of both *MleKlf5a* and *MleKlf5b* results in the diminution or loss of cell proliferation in endodermal stem cell niches and aberrant endodermal patterning. Our

results highlight an ancestral functional role for *Klf* transcription factors in the regulation of rapid cell proliferation in metazoan stem cell niches.

Main

Ctenophores are marine, invertebrate predators characterized by rows of giant cilia fused into 'ctenes' used for locomotion, an aboral and neuronal-rich gravity-sensing (apical) organ, and muscular tentacles lined with sticky colloblast cells used for prey capture [22–27]. *M. leidyi* embryos undergo a ctenophore-specific early cleavage program [28,29], gastrulation takes place ~3-5 hours post fertilization (hpf) followed by tissue organization and organogenesis over the course of the next several hours before hatching as cydippids ~18-22 hpf [30].

We used EdU incorporation assays to identify dividing cell populations during embryogenesis. EdU incorporation identified several regions during mid to late embryogenesis with rapid rates of cell proliferation (Fig. 1a-h). Four pairs of ctene rows, one pair in each quadrant, are typically among the first ectodermal structures to form [29]. Each ctene plate is made up of polster cells bearing fused giant cilia [31]. Beginning at 13 hpf, we observed EdU incorporation in a set of ectodermal cells surrounding each ctene row pair (Fig. 1b, f). In the pharynx, cell proliferation was initially widespread aborally during pharyngeal development and elongation (Fig. 1d). EdU incorporation in the pharynx subsequently becomes spatially restricted to two domains, one orally near the stomodeal opening, and the other aborally that includes the pharyngeal region forming the junction with the gastrovascular cavity (Fig. 1h). In the apical organ, cell proliferation was localized to the developing polar fields and a small subset of cells located deep within the epithelial floor along tentacular axis (Fig. 1a, e). Due to their proximity to where new lithocytes are formed, these deeper proliferative cells likely represent lithocyte progenitor cells [32].

62 Flanking the apical organ along the tentacular axis, ectodermal invaginations and internal
63 medial endodermal cell bands form the tentacle bulb organ [33–35] contributing to both the
64 ectodermal tentacular lateral ridges and the endodermal tentacular median ridges respectively,
65 each harboring progenitor cells that give rise to colloblasts and tentacle muscle [33–35]. During
66 tentacle bulb development EdU incorporation was initially observed in the median ridges (Fig.
67 1c-d). Later EdU incorporation was detected along the length of the median ridges and in the
68 lateral ridges (Fig. 1g-h). An Edu pulse followed by a 24 hour chase revealed that these
69 proliferative cells gave rise preferentially to tentacular muscle cells (Extended Data Fig. 1).
70 Previous cell proliferation studies in another ctenophore species, *Pleurobrachia pileus*, identified
71 gene expression indicative of 'stemness' such as *Piwi*, *Vasa*, *Nanos*, and *Sox* coincident with
72 EdU-positive cells in proliferative stem cell niches [15,19] similar to those observed during *M. leidyi*
73 embryogenesis.
74 The genome of *M. leidyi* contains three *Klf* genes: *MleKlf5a*, *MleKlf5b*, and *MleKlfX* [20].
75 *MleKlf5a* and *MleKlf5b* are the result of a lineage-specific duplication within the Ctenophora.
76 *MleKlfX* is highly derived with no clear orthology to any known metazoan *Klf* clade. *MleKlf5a*
77 and *MleKlf5b* transcripts are maternally loaded [21] and transcripts are detected in all embryonic
78 cells through gastrulation (Fig. 1i-l). Maternal loading has been observed in a number of *Klf*
79 genes among bilaterians [36–38]. Following gastrulation, *MleKlf5a* and *MleKlf5b* zygotic expression
80 is spatially localized to regions undergoing high rates of cell proliferation coincident with EdU
81 incorporation (Fig1 a-h, m-x). *MleKlf5a* and *MleKlf5b* expression overlap extensively in
82 endodermal domains during embryonic development (Fig. 1m-x). Interestingly a single
83 ectodermal expression domain unique to *MleKlf5b* is detected in proliferative cells flanking
84 developing ctene row polster cells (Fig. 1b, f, Extended Data Fig. 2a, b).

85 Within the pharynx, *MleKlf5a* and *MleKlf5b* expression is confined to the interior-most
86 cell layer. Expression in the aboral-most portion of the pharynx is associated with cells that form
87 the junction with the central gastrovascular cavity (infundibulum) and also throughout the
88 epithelial cell layer lining the developing infundibulum (Fig. 1n, p, r, t, v, x). During the initial
89 formation of the aboral apical organ, *MleKlf5a* and *MleKlf5b* expression is detected in the
90 epithelial floor. Subsequently, *MleKlf5a* and *MleKlf5b* expression in the apical organ becomes
91 restricted to cells that positionally correlate with putative lithocyte progenitors (Fig. 1r, t, v, x).
92 Within the developing tentacle bulbs, expression patterns of *MleKlf5a* and *MleKlf5b* mirror EdU
93 incorporation in regions of rapid cell proliferation (Fig. 1c-e, g-h, m-x). *MleKlf5a* and *MleKlf5b*
94 are highly expressed in the median ridge of developing tentacle bulbs (Fig. 1m-x), suggesting
95 that *MleKlf5a* and *MleKlf5b* may play a role in the maintenance of the median ridge tentacular
96 stem cell niche. In summary, *MleKlf5a* and *MleKlf5b* paralog expression extensively overlaps in
97 embryonic domains with high rates of cell proliferation. These regions express additional genes
98 associated with stemness such as *Piwi*, *Vasa*, *Nanos*, and *Sox* [11,15,16,19]. *MleKlf5a* and *MleKlf5b*
99 expression identifies putative stem cell niches within the aboral region of the pharynx, coincides
100 with putative lithocyte progenitor cells located in epithelial floor of the apical organ and
101 progenitor cells located in the median ridge of the tentacle bulb.

102 In contrast to *MleKlf5a* and *MleKlf5b* expression patterns, *MleKlfX* expression is
103 restricted to late stage embryos, first appearing ~16 hpf and does not appear to be associated with
104 EdU-positive cells (Extended Data Fig. 2c, d). *MleKlfX* expression is restricted to a small
105 number of cells within the apical organ. A deep set of *MleKlfX* expressing cells are located
106 centrally in the epithelial floor of the developing apical organ. A second shallower set is located
107 in each quadrant of the developing apical organ, just medial of the ciliated grooves. The two cell

108 clusters located along the tentacular plane are perpendicular to two additional cell clusters,
109 forming a cross-shaped pattern. These *MleKlfX* expressing cells positionally correspond with the
110 apical organ lamellate bodies, putative photoreceptor cells [39,40], suggesting that *MleKlfX* may
111 play a role in differentiation of light sensitive neuronal cell types in the apical organ. In
112 summary, *MleKlfX* a highly divergent gene in *M. leidyi*, appears to be expressed in a set of
113 differentiated neuronal cells, possibly involved with light sensing.

114 To characterize zygotic *Klf* gene function in *M. leidyi* we used both splice-blocking
115 morpholinos (sbMOs) and CRISPR-Cas9 genome editing to abrogate gene function during
116 embryonic development (Fig. 2). Knockdown of *MleKlfX* failed to produce any obvious
117 morphological phenotypes, so we focus here on the *MleKlf5a* and *MleKlf5b* results. It has been
118 shown that co-expressed KLFs bind to shared downstream regulatory targets resulting in
119 complex functional outcomes. For example, KLF2, KLF4, and KLF5 have redundant roles in the
120 downstream regulation of *Nanog* [4], whereas competition between KLF1 and KLF3 for binding
121 sites can result in differential functional outcomes [41]. For this reason we sought to maximize the
122 efficiency of generating an observable phenotype by performing simultaneous *MleKlf5a* and
123 *MleKlf5b* knockdown with both sbMO and CRISPR-Cas9 genome editing experiments. We
124 injected single-cell embryos with either *MleKlf5a*+*MleKlf5b* sbMOs or *MleKlf5a-*
125 *sgRNA*+*MleKlf5b-sgRNA*. Microinjected embryos were incubated to ~20 hpf and stained with
126 vital dyes (Fig. 3). Morphant and crispant specimens were imaged and compared to equivalent
127 late stage wildtype embryos from the same spawning events. A selection of morphants and
128 crispants were then subjected to single embryo RNA or DNA extractions respectively for gene
129 knockdown validation. Two sbMOs were designed for each gene (Fig. 2a, e). These produced
130 splice-blocking errors in morphants through exon skipping and/or intron retention (Fig. 2b, f).

131 An initial set of 4 sgRNAs were designed for *MleKlf5a* and *MleKlf5b* (Table 1) based on the *M.*
132 *leidyi* reference genome [24, 49]. A single sgRNA for each gene, *MleKlf5a-sgRNA4* and *MleKlf5b-*
133 *sgRNA3*, proved efficient at mediating Cas9 double-stranded break activity at the target loci (Fig.
134 2c-d, g-h). Sanger sequencing followed by ICE analysis revealed clear degradation of signal in
135 the crispants at the target loci compared to control embryos (Fig. 2c,g), indicating *MleKlf5a-*
136 *sgRNA4* and *MleKlf5b-sgRNA3* targeted Cas9 exonuclease activity produced indels and
137 frameshift mutations (Extended Data Fig. 3b). Control injections with a standard control MO,
138 Cas9 protein alone, and sgRNAs alone had no detectable effect on embryonic development
139 (Extended Data Fig. 3a). No evidence of off-target Cas9 activity was observed in tested loci
140 (Table 2) thus phenotypes generated via both double gene abrogation approaches in our study
141 were due to the disruption of *MleKlf5a* and *MleKlf5b* activity.

142 Both *MleKlf5a+MleKlf5b* morphants and crispants generated an allelic series of
143 phenotypes (Fig. 3a-p). While morphants and crispants phenocopied one another, a higher
144 proportion of severe phenotypes were observed among cripsants as compared to morphants as
145 expected (Fig. 3s) reflecting the effects of Cas9 mediated genome editing versus titration of
146 functional mRNAs by sbMOs. In contrast to the observation of primarily severe phenotypes in
147 the crispant *MleKlf5a-sgRNA4+MleKlf5b-sgRNA3* double gene knockdowns (Fig. 3o-p; Fig. 4e-
148 f, l-m), single gene knockdown with either *MleKlf5a-sgRNA4* or *MleKlf5b-sgRNA3* generated
149 predominantly mild phenotypes (Extended Data Fig. 4). This suggests that *MleKlf5a* and
150 *MleKlf5b* likely have functionally redundant regulatory roles in maintaining proliferative
151 endodermal stem cell niches during embryonic development. Further investigation will be
152 needed to determine whether *MleKlf5a* and *MleKlf5b* are acting on the same direct downstream
153 targets, or acting indirectly on complementary non-overlapping sets of genes regulating cell

154 proliferation. For example, in mouse embryonic stem cells, pluripotency and proliferation are
155 maintained through differential inhibition of endoderm and mesoderm by *Klf4* and *Klf5*
156 respectively [42]. With regard to the unique ectodermal expression domain of *MleKlf5b*, no
157 ectodermal or ctene row phenotype was observed in *MleKlf5b-sgRNA3* or *MleKlf5a-sgRNA4*
158 crispants nor double gene abrogation experiments. Ctenes are initially established by maternal
159 factors [29], new polster cells and ctene row expansion begin post-hatching in the cydippid stage [43].
160 Thus the observed EdU- and *MleKlf5b*-positive ectodermal cells (Fig. 1b, f: Extended Data Fig.
161 2a-b) likely contribute to ctene row expansion post-hatching and/or perhaps also play a role in
162 the growth and maintenance of surrounding ectodermal epithelia post-hatching.

163 Embryos with mild phenotypes underwent pharyngeal elongation concomitant with
164 mesogleal deposition and an increase in size; however, they displayed disorganized endodermal
165 patterning associated with the aboral end of the pharynx and infundibular gastrovascular cavity
166 (Fig. 3e-f, m-n). In some cases we observed instances of pharyngeal bifurcation at the junction
167 with the gastrovascular cavity (Fig. 3 f,n; Extended Data Fig. 4b; Extended Data Fig. 5). In
168 contrast, embryos classified as having severe phenotypes (Fig. 3g-h, o-p) failed to increase in
169 size, likely reflecting a lack of ECM extrusion into the mesogleal space, resulting in internal
170 embryonic spaces being disproportionately occupied by gastrovascular endoderm and a failure of
171 normal pharyngeal elongation. Assessment of cell proliferation in *MleKlf5a-sgRNA4+MleKlf5b-*
172 *sgRNA3* crispants revealed a dramatic reduction of EdU incorporation at the aboral end of the
173 pharynx (Fig. 3q, r). These results suggest that zygotic *MleKlf5a* and *MleKlf5b* play a
174 coordinated role in the growth and patterning of the gastrovascular cavity and pharynx,
175 particularly at the pharyngeal gastrovascular junction, presumably through maintenance of cell
176 proliferation in putative endodermal stem cell niches in these tissues.

177 Across both morphants and crispants, additional patterning defects were observed in the
178 apical organ epithelial floor and in the tentacle bulbs (Fig. 3; Fig. 4). *MleKlf5a* and *MleKlf5b*
179 knockdown resulted in a significant reduction of apical organ lithocytes as compared to control
180 embryos (Fig. 4a-g). By 20 hpf, control embryo statocysts contain ~7 lithocytes (Fig. 4a-b, g).
181 *MleKlf5a+MleKlf5b* morphants had an average ~4 lithocytes (Fig. 4g), with three lacking
182 lithocytes entirely (Fig. 4c, d). *MleKlf5a-sgRNA4+MleKlf5b-sgRNA3* crispants had an average of
183 ~2 lithocytes (Fig. 4g), with five completely lacking lithocytes (Fig. 4e, f). In embryos lacking
184 lithocytes, both balancer cilia and dome cilia were present (Fig. 4d, f), reflecting that lithocytes
185 are derived from endoderm while the balancer and dome cilia are derived from ectoderm [34]. This
186 suggests that *MleKlf5a* and *MleKlf5b* play a role in maintenance of endodermally derived
187 lithocyte progenitor cells in the apical organ.

188 Simultaneous abrogation of *MleKlf5a* and *MleKlf5b* also resulted in a dramatic reduction
189 in tentacle bulb size, particularly notable in the tentacular median ridge (Fig. 4h-n). We
190 measured the length of the tentacular median ridge and found significant differences between
191 control and injected embryos (Fig. 4n; Extended Data Fig. 6). In control embryos the tentacular
192 median ridge was, on average, 23 µm in length, whereas in *MleKlf5a+MleKlf5b* morphants and
193 *MleKlf5a-sgRNA4+MleKlf5b-sgRNA3* crispants, the average tentacular median ridge length was
194 ~18 µm and ~9 µm respectively (Fig. 4n). Furthermore, we observed that 15% of the
195 *MleKlf5a+MleKlf5b* morphants and 29% of the *MleKlf5a-sgRNA4+MleKlf5b-sgRNA3* crispants
196 lacked tentacular median ridges altogether (Fig. 4j-m). Assessment of cell proliferation in
197 *MleKlf5a-sgRNA4+MleKlf5b-sgRNA3* crispants revealed a dramatic reduction in EdU
198 incorporation in the tentacular median ridges, but not in the tentacular lateral ridges (Fig. 3q, r).
199 This indicates that proliferation in the tentacular lateral ridge stem cell niches were largely

200 unaffected in both morphants and crispants. Lateral ridge stem cells give rise to tentacle epithelia
201 and colloblasts [15,35], which were present in embryos with reduced median ridges (Fig. 4j-m). Our
202 results support a requirement for *MleKlf5a* and *MleKlf5b* activity for normal tentacle bulb
203 development and specifically for production of tentacle root muscle through maintenance of cell
204 proliferation in the endodermally-derived tentacular median ridge stem cell niche.

205 In this study, we used both sbMOs and Cas9-mediated genome editing to coordinately
206 abrogate zygotic *MleKlf5a* and *MleKlf5b* gene function during *M. leidyi* embryonic development.
207 We show that Cas9-mediated genome editing is an effective method for performing
208 combinatorial gene function assays in F0 ctenophore embryos. Along with recent RNA-seq data
209 highlighting candidate genes associated with zygotic gene activation and specific cell types in
210 ctenophores [21,35,44], sbMO and CRISPR-Cas9 based gene function assays in *M. leidyi* will
211 provide much needed insight into the genetic underpinnings of ctenophore biology and further
212 our understanding of early metazoan evolution. Our results highlight an essential role for zygotic
213 *MleKlf5a* and *MleKlf5b* activity in promoting cell proliferation in tissue and organ specific stem
214 cell niches that remain active throughout the lifespan of *M. leidyi* that produce a number of
215 terminally differentiated cell types unique to the Ctenophora. Our results further suggest that the
216 functional activity of *Klfs* in promoting cell proliferation within stem cell niches represents a
217 conserved ancestral function of this gene family across the Metazoa.
218

219 **Fig. 1: *MleKlf5a* and *MleKlf5b* are expressed in regions of rapid cell proliferation during**
220 **embryogenesis in *Mnemiopsis leidyi.*** Schematic depiction of tentacular axis (TA) and
221 pharyngeal axis (PA) orientation are located in panel upper right. Aboral view in **a, c, e, g, j, l,**
222 **m, o, q, s, u, w**. Lateral view, oral up, in **b, d, f, h, k, n, p, r, t, v, x**. Scale bars are 50 µm. (**a-h**)

223 25 min EdU pulse in 13 hours post fertilization (hpf) (**a-d**) and 16 hpf (**e-h**) embryos. EdU
224 incorporation is localized to two cell clusters in the apical organ (**a, e**), epithelial cells flanking
225 the developing ctene rows (bounded by dashed lines) (**b, f**), epithelial cells lining the
226 gastrovascular cavity (gvc) (**d, h**) in the developing tentacular median ridges (arrowheads), and
227 the oral (oph) and aboral (aph) regions of the pharynx (**d**). (**g, h**) Later in development, EdU
228 incorporation is found in the tentacular median ridge (arrowheads) and lateral ridges (lr) of the
229 tentacle bulbs and in both oral (oph) and aboral (aph) regions of the pharynx. (**i-x**) mRNA
230 expression patterns for *MleKlf5a* and *MleKlf5b* during embryogenesis. Maternal transcripts for
231 both *MleKlf5a* (**i, j**) and *MleKlf5b* (**k, l**) are found ubiquitously in zygotes (**i**), early cleavage
232 stages (**k**) and gastrulae (**j, l**). (**m-p**) Zygotic *MleKlf5a* and *MleKlf5b* transcripts exhibit
233 overlapping endodermal expression domains. At 9 hpf expression of *MleKlf5a* and *MleKlf5b*
234 transcripts are localized to the forming tentacular median ridges (arrowheads) and the developing
235 pharynx (oph + aph). (**q-t**) At 14 hpf *MleKlf5a* and *MleKlf5b* transcript expression is also found
236 in the apical organ (arrows) and epithelia of the newly formed gastrovascular cavity (gvc). (**u-x**)
237 At 20 hpf *MleKlf5a* and *MleKlf5b* transcripts are found in the tentacular median ridge
238 (arrowheads) and lateral ridge (lr), on either side of the apical organ floor (arrows), localized
239 towards the aboral end of the pharynx (aph), and the gastrovascular cavity epithelium (gvc).
240

241 **Fig. 2: Two independent methods used to abrogate *MleKlf5a* and *MleKlf5b* gene function.**
242 *MleKlf5a* (**a**) and *MleKlf5b* (**e**) exon-intron schematics show the location of sbMO targets (blue
243 boxes) and sgRNA targets (black triangle) used in this study. (**b,f**) Electrophoretic gels of PCR
244 products obtained using *MleKlf5a* and *MleKlf5b* sbMO RT-PCR primers (arrows in predicted
245 spliceform schematics to the right) on cDNA obtained from an individual morphant exemplar (*n*

246 = 21 morphants), 2-log DNA ladder was used for band size reference. Wildtype (wt) and mis-
247 spliced transcripts due to exon-skipping (-E) and/or intron retention (+I) were present in
248 morphants. (**c-d, g-h**) Crispant discordance plots and corresponding Sanger sequence traces.
249 sgRNA target site is underlined, Cas9 cut site is represented by dashed line and shows clearly
250 elevated sequence discordance relative to genome sequence reference and control sanger
251 sequencing. Sanger sequencing signal degradation is caused by the introduction of indels in an
252 individual crispant exemplar (*n* = 17 crispants; also see **EDF3b**).
253
254 **Fig. 3: *MleKlf5a* and *MleKlf5b* double gene knockdown via sbMO and *sgRNA*-Cas9 genome**
255 **editing.** (**a-p**) Live imaging showing morphology of 20 hpf cydippids. Aboral view in **a, c, e, g,**
256 **i, k, m, o**. Lateral view, oral up, in **b, d, f, h, j, l, n, p, q, r**. Schematic depiction of tentacular
257 axis (TA) and pharyngeal axis (PA) orientation are located in panel upper right. Scale bars are 50
258 µm. Hoechst (blue) marks nuclei. Mitotracker (red) preferentially marks position of ctene row
259 polster cells, one pair per embryonic quadrant. Lysotracker (yellow) preferentially stains
260 epithelial cells lining the gastrovascular cavity (gvc). Tentacular median ridges (arrowheads) are
261 positioned medially along the tentacular axis and contacted by gvc epithelial cells. The pharynx
262 (ph) is positioned centrally and joins with the gvc aborally. The apical organ (arrow) is located at
263 the aboral pole of the embryo. Un-injected wildtype embryo (**a, b**). Morphology is unaffected in
264 embryos sham injected with control morpholino (MO) (**c, d**), *sgRNA* only (**i, j**) or Cas9 protein
265 only (**k, l**). In contrast, mild phenotypes in double gene knockdown morphants (**e, f**) and double
266 gene edited crispants (**m, n**) display aberrant distributions of gvc epithelial cells (Lysotracker
267 signal), aberrant patterning of the pharynx (ph) including aboral bifurcations (**f**, **n**, **EDF4**,
268 **EDF5**), aberrant patterning of the tentacle bulb and tentacular median ridges (arrowheads), and

269 atypical apical organ (arrow) morphology. Severe phenotypes in double gene knockdown
270 morphants (**g, h**) and double gene edited crispants (**o, p**) are reduced in size due to lack of
271 mesogleal ECM extrusion, display collapsed pharynx with gvc junction defects, significantly
272 reduced tentacle bulbs and tentacular median ridges (arrowheads), and apical organ defects
273 (arrow). (**q**) 25 min EdU pulse in wildtype 16 hpf embryo. Strong EdU incorporation signal
274 (orange) is found in the oral (oph) and aboral (aph) regions of the developing pharynx, epithelial
275 cells lining the gastrovascular cavity (gvc), the developing tentacular median ridges (arrowheads)
276 and lateral ridges (lr) of the tentacle bulbs. (**r**) 25 min EdU pulse in 16 hpf crispant embryo. EdU
277 incorporation signal (orange) is significantly diminished in regions that also express *MleKlf5a*
278 and *MleKlf5b* (refer to **Fig. 1**) including the pharynx, gvc and tentacular median ridges. Note that
279 lr cell proliferation is not affected. (**s**) Comparison of phenotypic proportions in morphants (n =
280 45) (51% no phenotype, 29% mild phenotype, 20% severe phenotype) vs crispants (n = 16) (6%
281 no phenotype, 19% mild phenotype, 75% severe phenotype).
282
283 **Fig. 4: *MleKlf5a* and *MleKlf5b* double gene knockdown negatively affects apical organ**
284 **lithocyte production and negatively affects tentacular median ridge size.** Live images of
285 embryos at 20 hpf. Schematic depiction of tentacular axis (TA) and pharyngeal axis (PA)
286 orientation are located in panel upper right. Aboral view in **a, c, e, h, j, l**. Lateral view, oral up, in
287 **b, d, f, i, k, m**. Scale bars are 50 µm. (**a, b**) lithocytes (arrow), dome cilia (arrowhead) and apical
288 organ (ao) in wildtype embryo. (**c, d**) double gene knockdown morphant lacking lithocytes. (**e, f**)
289 double gene edited crispant lacking lithocytes. Dome cilia (arrowheads) and balancer cilia are
290 present in both morphants and crispants. (**g**) *MleKlf5a* and *MleKlf5b* double gene knockdown
291 significantly reduces lithocyte production. Box plot center lines show medians, box limit at 25th

292 and 75th percentiles, whiskers extend 1.5 times interquartile range from the 25th and 75th
293 percentiles, data points are plotted as open circles. * = two-tailed t-test, t = 3.47, P<0.005. ** =
294 two-tailed t-test, t = 6.52, P<0.00001. Wildtype (n = 14), morphant (n = 33), crispant (n = 15).
295 (**h, i**) Wildtype tentacular median ridge (arrowhead) and lateral ridge (lr). (**j, k**) double gene
296 knockdown morphant with dramatically reduced tentacular median ridge. (**l, m**) double gene
297 edited crispant with dramatically reduced tentacular median ridge. The tentacle bulb lateral ridge
298 remains present in both morphants and crispants. (**n**) *MleKlf5a* and *MleKlf5b* double gene
299 knockdown significantly reduces tentacular median ridge length. Box plot center lines show the
300 median, box limit at 25th and 75th percentiles, whiskers extend 1.5 times interquartile range
301 from the 25th and 75th percentiles, data points are plotted as open circles. * = two-tailed t-test, t
302 = 4.01, P<0.0005. ** = two-tailed t-test, t = 8.32, P<0.00001. Each data point represents a
303 single tentacular median ridge length, with a maximum of 2 data points (i.e., 2 tentacular median
304 ridges) from each embryo. Data value of 0 indicate the absence of a tentacular median ridge
305 and/or tentacle bulb. Wildtype (n = 28), morphant (n = 61), crispant (n = 34).
306
307 **Extended Data Fig. 1: Proliferating cells in the tentacular median ridge give rise to tentacle**
308 **muscle in *M. leidyi*.** Aboral view and schematic depiction of tentacular axis (TA) and
309 pharyngeal axis (PA) orientation are located in panel upper right. Scale bars are 50 µm. EdU
310 pulse:chase immunohistochemistry on tentacle bulbs (**a**) after 25 min pulse:0 min chase and (**b**)
311 after 25 min pulse:24 hr chase. (**a**) 25 min pulse EdU marks rapidly proliferating cells in the
312 tentacular median ridge (arrow) and lateral ridges (lr) of the tentacle bulb. (**b**) After 25 min
313 pulse:24 hr chase, EdU incorporation is primarily detected in emergent tentacle muscle cells.
314

315 **Extended Data Fig. 2: Additional *MleKlf5b* and *MleKlfX* transcript expression domains.**
316 Schematic depiction of tentacular axis (TA) and pharyngeal axis (PA) orientation are located in
317 panel upper right. Scale bars are 50 µm. (**a, b**) 9 hpf and 14 hpf embryos, lateral view, oral up.
318 Dashed lines bound *MleKlf5b* ectodermal expression (magenta) in rapidly dividing cells
319 (compare with **Fig. 1b, f**) that flank developing ctene row pairs (visible as aligned columns of
320 DAPI stained nuclei bounded by *MleKlf5b* expression). (**c, d**) Magnified aboral views of
321 *MleKlfX* expression (magenta) in epithelial floor cells of the apical organ. (**c**) Initially *MleKlfX*
322 expression is detected at 16 hpf in four small clusters of cells at the boundary of each developing
323 embryonic quadrant converging in the center of the apical organ. (**d**) Expression of *MleKlfX*
324 resolves into several cell clusters by 18 hpf in both the tentacular (TA) and pharyngeal (PA)
325 axes.
326
327 **Extended Data Fig. 3: ICE analysis of Crispants.** (**a**) Sham injection has no effect on
328 embryonic development. Bar graph comparison of percentage of normal development in
329 wildtype n = 161 (24 abnormal); devitellinized but uninjected n = 217 (42 abnormal), two-tailed
330 Fisher's exact test P=0.2761; control MO injected n = 49 (10 abnormal), two-tailed Fisher's
331 exact test P=0.379; Cas9 only injected n = 7 (1 abnormal), two-tailed Fisher's exact test P=1;
332 sgRNA only injected n = 4 (1 abnormal), two-tailed Fisher's exact test P=0.4851. (**b**)
333 Distribution of ICE scores (estimate of indel proportion in signal trace from genomic DNA of
334 individual crispants) and KO scores (estimate of indel proportion that result in frameshift
335 mutation) for *MleKlf5a-sgRNA4* (n = 14) and *MleKlf5b-sgRNA3* (n = 17). Cas9 cut sites were
336 PCR amplified from genomic DNA prepared from individual crispants and subsequently Sanger
337 sequenced. Each cut site data point represents Sanger trace analyses from an individual embryo.

338 Box plot center lines show the median, box limit at 25th and 75th percentiles, whiskers extend
339 1.5 times interquartile range from the 25th and 75th percentiles, data points are plotted as open
340 circles.
341
342 **Extended Data Fig. 4: Cas9 mediated genome editing of either *MleKlf5a* or *MleKlf5b***
343 **resulted in reduced phenotype penetrance.** Schematic depiction of tentacular axis (TA)
344 orientation located in panel upper right. Lateral view, oral up, scale bars are 50 µm. Single gene
345 editing produced primarily mild phenotypes for both *MleKlf5a* crispants (**a**) and *MleKlf5b*
346 crispants (**b**). (**c**) Bar graph comparison of distribution of mild (gray) vs severe (black)
347 phenotypes in *MleKlf5a* crispants (n = 5, 80% mild) and *MleKlf5b* crispants (n = 5, 80% mild).
348
349 **Extended Data Fig. 5: Aberrant pharyngeal patterning.** Schematic depiction of tentacular
350 axis (TA) and pharyngeal axis (PA) orientation located in panel upper right. Lateral views, oral
351 up, scale bars are 50 µm. (**a, b**) 20 hpf double gene morphant embryo with bifurcated (arrow)
352 pharynx (ph). (**c, d**) Same individual morphant 3 days post fertilization (dph) showing
353 persistence of pharyngeal bifurcation patterning defect just anterior of the pharyngeal-
354 gastrovascular junction resulting in a deletion of the pharyngeal folds.
355
356 **Extended Data Fig. 6: Schematic of cydippid tentacle bulb.** Aboral top, lateral bottom.
357 Tentacular median ridge colored light gray. Tentacular lateral ridges colored darker gray.
358 Tentacle (not shown) is rooted at the aboral medial base of the tentacle bulb. Location of
359 measurement taken for the tentacular median ridge length (refer to **Fig. 4n**) is denoted with red
360 dashed line.

361

362 **Methods**

363 **Cloning and *in situ* hybridization**

364 RNA was extracted using Trizol (Thermo Fisher Scientific) from *Mnemiopsis* embryos
365 collected at different stages of development and used to generate cDNA libraries (SMARTer kit,
366 Clontech). The coding sequences of *MleKlf5a*, *MleKlf5b*, and *MleKlfX* were amplified from
367 cDNA (Table 1) and cloned into pGEM-T Easy vector (Promega). The cloned fragments were
368 used as templates for *in vitro* transcription (MEGAscript, Ambion) of antisense digoxigenin-
369 labeled (Digoxigenin-11-UTP, Roche) riboprobes.

370 *In situ* hybridization followed ([46]). Riboprobes were used at a final concentration of ~0.5
371 ng/µl and hybridized with embryos for 24 hours. After color development, nuclei were labeled
372 with either DAPI (Molecular Probes) or Hoechst 33342 (Molecular Probes) in 1x PBS. Embryos
373 were immediately imaged or stored at -20°C in 70% glycerol in 1x PBS. Images were acquired
374 using a Zeiss Axio Imager.Z2, Zeiss AxioCam MRm Rev3 camera, and Zeiss Zen Blue software.
375 Fluorescent Z-stacks were deconvolved, post-processed for brightness and contrast and
376 assembled in Adobe Photoshop. Monochrome brightfield images were inverted, pseudocolored,
377 and overlaid onto fluorescent images of labeled nuclei. Samples were stored at -20°C in 70%
378 glycerol in 1x PBS.

379

380 **Vital Dye staining**

381 Live embryos were incubated in filtered seawater (FSW) containing a final concentration
382 of 100 nM MitoTracker (Deep Red FM, Molecular Probes), 100 nM LysoTracker (Red DND-99,
383 Molecular Probes), and 10 ng/µl Hoechst 33342 for one hour at room temperature. Live embryos

384 were then placed on glass microscope slides in a drop of FSW and relaxed with a drop of 6.5%
385 $MgCl_2$ (in dH_2O) on a coverslip positioned with clay feet. Images were acquired using a Zeiss
386 Axio Imager.Z2, Zeiss AxioCam MRm Rev3 camera, and Zeiss Zen Blue software. Fluorescent
387 Z-stacks were deconvolved, post-processed for brightness and contrast, and assembled in Adobe
388 Photoshop.
389
390 **EdU labeling**
391 Click-iT® EdU Alexa Fluor® 647 Imaging Kit (ThermoFisher Scientific) was used for
392 identification of proliferating cells. Embryos were collected at different developmental stages
393 and pulse incubated for 25 minutes with 100 µM EdU in a solution of a 1:1 volumetric ratio of
394 FSW to 6.5% $MgCl_2$ (dissolved in dH_2O) at room temperature. The EdU solution was washed
395 out and embryos were either fixed immediately or allowed to continue to develop during a 24
396 hour chase and subsequently fixed. Embryos were fixed with 4% PFA:FSW for 30 minutes at
397 room temperature, washed with 3% BSA:1xPBS), and incubated with 0.5% Triton X-100:1x
398 PBS for 20 minutes at room temperature. Fixed embryos were washed with 3% BSA:1x PBS and
399 stored at 4°C until used for EdU detection as per manufacturer protocol. Embryos were
400 subsequently washed with 1x PBS and mounted on glass microscope slides. Images were
401 acquired using a Zeiss Axio Imager.Z2, Zeiss AxioCam MRm Rev3 camera, and Zeiss Zen Blue
402 software. Fluorescent Z-stacks were deconvolved, post-processed for brightness and contrast,
403 and assembled in Adobe Photoshop or FIJI [47].
404
405 **Microinjection**

406 Laboratory cultures of adult *Mnemiopsis leidyi* on a ~12 hr:12 hr light:dark cycle were
407 spawned ~4 hours post darkness (hpd). At ~3.5 hpd individual adult *M. leidyi* were placed into 8-
408 inch glass bowls and screened for mature sperm and eggs. Freshly fertilized eggs were collected
409 by pipette.

410 Microinjection needles were pulled with a Brown micropipette puller (P-1000, Sutter
411 Instrument Company) using aluminosilicate glass capillaries (AF100-64-10, Sutter Instrument
412 Company). Pulled capillaries were beveled using a microelectrode beveler (BV-10, Sutter
413 Instrument Company). Beveled capillary needles were loaded via backfilling with injection
414 cocktails mixed with fluorescently-conjugated dextran (Invitrogen) (used to assess injection
415 success). Loaded capillary needles were mounted to a Xenoworks microinjection system (Sutter
416 Instrument Company) paired to a Zeiss Discovery V8 epiflourescent stereomicroscope.

417 Fertilized *M. leidyi* eggs were collected and passed sequentially through a 500 µm and a
418 400 µm cell strainer (pluriSelect Life Science) to remove excess mucus and egg jelly. Embryos
419 were then washed with 1x Penicillin/Streptomycin:FSW (PS:FSW). The embryonic vitelline
420 membranes were removed in gelatin coated dishes with acid-sharpened tungsten needles.
421 Embryos were then carefully transferred to an injection dish. After microinjection, embryos were
422 kept at room temperature until reaching the desired development stage for further analyses.

423 To determine if removing the vitelline membrane had an effect on embryogenesis, we
424 scored the percentage of normal development in embryos that were removed from the vitelline
425 membrane but not injected. There was no significant difference in the percentage of normal
426 development between embryos kept in their vitelline membrane (85%, n=161) and those that
427 were devitellinized but uninjected (80%, n=217; $\square^2$=1.5272, p=0.217; Extended Data Fig. 3a).
428

429 **Morpholino oligonucleotides**

430 Splice-blocking morpholino oligonucleotides (sbMOs, Gene Tools) were designed for
431 both *MleKlf5a* (*ML00922a*) and *MleKlf5b* (*ML25776a*). *MleKlf5a* sbMO #1 and sbMO #2
432 targeted intron 2-exon 3 and intron 3-exon 4 boundaries, respectively. *MleKlf5b* sbMO #1 and
433 sbMO #2 targeted exon 6-intron 6 and exon 7-intron 7 boundaries, respectively. A standard
434 control MO was used as a negative control. Sequences of sbMOs are listed in Table 1. Stock
435 solutions of sbMO in dH_2O were stored at room temperature. sbMO injection cocktail solutions
436 consisted of a final sbMO concentration of ~333 nM and ~0.5 mg/ml fluorescent dextran
437 (rhodamine or Alexa-Fluor 488, 10,000 MW, Invitrogen) in 35% glycerol. After phenotypic
438 analyses RNA was extracted from individual embryos (Arcturus PicoPure, ThermoFisher) and
439 cDNA prepared. Gene-specific primers were used on cDNA (OneTaq One-Step RT-PCR, New
440 England Biolabs) to evaluate aberrant transcript splicing via gel electrophoresis.

441

442 **CRISPR/Cas9**

443 We followed a cloning-free method to generate sgRNAs [48,49]. PCR amplified templates
444 were generated by annealing a 20-nt universal tracrRNA oligo to a sgRNA-specific oligo that
445 consisted of a T7 promoter, followed by the sgRNA target sequence, and a complementary
446 sequence to the tracrRNA oligo (Table 1). These templates were then *in vitro* transcribed
447 (MEGAscript, Ambion) to generate sgRNAs. The CasOT program [50] and *M. leidyi* reference
448 genome [51] were used to identify sgRNA target sites for *MleKlf5a* (*ML00922a*), *MleKlf5b*
449 (*ML25776a*), and *MleKlfX* (*ML20061a*). We selected sgRNAs that had no fewer than four
450 mismatches to alternative genomic sites to minimize potential off-target site (OTS) activity
451 (Table 1). Recombinant Cas9 protein (PNA Bio) and sgRNAs were injected at concentrations of

452 400 ng/µl of Cas9 protein and 100 ng/µl for each sgRNA. After phenotypic analysis, genomic
453 DNA was extracted from individual embryos (QIAamp DNA Micro, Qiagen) and each sgRNA
454 target site was amplified and Sanger sequenced. The ICE analysis tool (Synthego,
455 https://ice.synthego.com/#/) was used to determine Cas9 efficiency for each sgRNA. ICE
456 analysis gives two scores: an ICE score which reflects the percentage of indels found and a KO
457 score which reflects the percentage of indels that produce a frameshift mutation.
458

459 **References**

460 1. Takahashi, K. & Yamanaka, S. Induction of pluripotent stem cells from mouse embryonic
461 and adult fibroblast cultures by defined factors. *Cell* **126,** 663–676 (2006).
462 2. Takahashi, K. *et al.* Induction of pluripotent stem cells from adult human fibroblasts by
463 defined factors. *Cell* **131,** 861–872 (2007).
464 3. Rosselló, R. A. *et al.* Mammalian genes induce partially reprogrammed pluripotent stem
465 cells in non-mammalian vertebrate and invertebrate species. *eLIFE* **2,** e00036 (2013).
466 4. Jiang, J. *et al.* A core Klf circuitry regulates self-renewal of embryonic stem cells. *Nat. Cell*
467 *Biol.* **10,** 353–360 (2008).
468 5. Parisi, S. *et al.* Direct targets of Klf5 transcription factor contribute to the maintenance of
469 mouse embryonic stem cell undifferentiated state. *BMC Biol.* **8,** 128 (2010).
470 6. McConnell, B. B. & Yang, V. W. Mammalian Krüppel-like factors in health and diseases.
471 *Physiol. Rev.* **90,** 1337–1381 (2010).
472 7. Parisi, S. *et al.* Klf5 is involved in self-renewal of mouse embryonic stem cells. *J. Cell Sci.*
473 **121,** 2629–2634 (2008).
474 8. Nandan, M. O. & Yang, V. W. The role of Krüppel-like factors in the reprogramming of

475 somatic cells to induced pluripotent stem cells. *Histol. Histopathol.* **24,** 1343–1355 (2009).

476 9. Nandan, M. O., Ghaleb, A. M., Bialkowska, A. B. & Yang, V. W. Krüppel-like factor 5 is
477 essential for proliferation and survival of mouse intestinal epithelial stem cells. *Stem Cell*
478 *Res.* **14,** 10–19 (2015).

479 10. Steele, R. E., David, C. N. & Technau, U. A genomic view of 500 million years of cnidarian
480 evolution. *Trends Genet.* **27,** 7–13 (2011).

481 11. Schnitzler, C. E., Simmons, D. K., Pang, K., Martindale, M. Q. & Baxevanis, A. D.
482 Expression of multiple *Sox* genes through embryonic development in the ctenophore
483 *Mnemiopsis leidyi* is spatially restricted to zones of cell proliferation. *Evodevo* **5,** 15 (2014).

484 12. Dunn, C. W. *et al.* Broad phylogenomic sampling improves resolution of the animal tree of
485 life. *Nature* **452,** 745–749 (2008).

486 13. Hejnol, A. *et al.* Assessing the root of bilaterian animals with scalable phylogenomic
487 methods. *Proc. Biol. Sci.* **276,** 4261–4270 (2009).

488 14. Whelan, N. V. *et al.* Ctenophore relationships and their placement as the sister group to all
489 other animals. *Nat Ecol Evol* (2017). doi:10.1038/s41559-017-0331-3

490 15. Alié, A. *et al.* Somatic stem cells express *Piwi* and *Vasa* genes in an adult ctenophore:
491 Ancient association of 'germline genes' with stemness. *Dev. Biol.* **350,** 183–197 (2011).

492 16. Reitzel, A. M., Pang, K. & Martindale, M. Q. Developmental expression of 'germline'- and
493 'sex determination'-related genes in the ctenophore *Mnemiopsis leidyi*. *Evodevo* **7,** 17
494 (2016).

495 17. Martindale, M. Q. The ontogeny and maintenance of adult symmetry properties in the
496 ctenophore, *Mnemiopsis mccradyi*. *Dev. Biol.* **118,** 556–576 (1986).

497 18. Martindale, M. Q. The onset of regenerative properties in ctenophores. *Curr. Opin. Genet.*

498 *Dev.* **40,** 113–119 (2016).

499 19. Jager, M., Quéinnec, E., Chiori, R., Le Guyader, H. & Manuel, M. Insights into the early
500 evolution of SOX genes from expression analyses in a ctenophore. *J. Exp. Zool. B Mol.*
501 *Dev. Evol.* **310,** 650–667 (2008).

502 20. Presnell, J. S., Schnitzler, C. E. & Browne, W. E. KLF/SP Transcription Factor Family
503 Evolution: Expansion, Diversification, and Innovation in Eukaryotes. *Genome Biol. Evol.* **7,**
504 2289–2309 (2015).

505 21. Davidson, P. L. *et al.* The maternal-zygotic transition and zygotic activation of the
506 *Mnemiopsis leidyi* genome occurs within the first three cleavage cycles. *Mol. Reprod. Dev.*
507 (2017). doi:10.1002/mrd.22926

508 22. Chun, C. *Die ctenophoren des Golfes von Neapel und der angrenzenden meeres-abschnitte*.
509 (W. Engelmann, 1880).

510 23. von Byern, J., Mills, C. E. & Flammang, P. Bonding tactics in ctenophores—morphology
511 and function of the colloblast system. in *Biological Adhesive Systems: From Nature to*
512 *Technical and Medical Application* (eds. von Byern, J. & Grunwald, I.) 29–40 (Springer,
513 2010).

514 24. Ryan, J. F. *et al.* The genome of the ctenophore *Mnemiopsis leidyi* and its implications for
515 cell type evolution. *Science* **342,** 1242592 (2013).

516 25. Moroz, L. L. *et al.* The ctenophore genome and the evolutionary origins of neural systems.
517 *Nature* **510,** 109–114 (2014).

518 26. Tamm, S. L. Cilia and the life of ctenophores. *Invertebr. Biol.* **133,** 1–46 (2014).

519 27. Pang, K. & Martindale, M. Q. Ctenophores. *Curr. Biol.* **18,** R1119–20 (2008).

520 28. Freeman, G. The effects of altering the position of cleavage planes on the process of

521 localization of developmental potential in ctenophores. *Dev. Biol.* **51,** 332–337 (1976).

522 29. Fischer, A. H., Pang, K., Henry, J. Q. & Martindale, M. Q. A cleavage clock regulates
523 features of lineage-specific differentiation in the development of a basal branching
524 metazoan, the ctenophore *Mnemiopsis leidyi*. *Evodevo* **5,** 4 (2014).

525 30. Pang, K. & Martindale, M. Q. Comb Jellies (Ctenophora): A Model for Basal Metazoan
526 Evolution and Development. *CSH Protoc.* **2008,** db.emo106 (2008).

527 31. Tamm, S. L. Mechanisms of Ciliary Co-Ordination in Ctenophores. *J. Exp. Biol.* **59,** 231–
528 245 (1973).

529 32. Tamm, S. L. Formation of the statolith in the ctenophore *Mnemiopsis leidyi*. *Biol. Bull.* **227,**
530 7–18 (2014).

531 33. Martindale, M. Q. & Henry, J. J. Experimental Analysis of Tentacle Formation in the
532 Ctenophore *Mnemiopsis leidyi*. *Biol. Bull.* **193,** 245–247 (1997).

533 34. Martindale, M. Q. & Henry, J. Q. Intracellular fate mapping in a basal metazoan, the
534 ctenophore *Mnemiopsis leidyi*, reveals the origins of mesoderm and the existence of
535 indeterminate cell lineages. *Dev. Biol.* **214,** 243–257 (1999).

536 35. Babonis, L. S. *et al.* Integrating embryonic development and evolutionary history to
537 characterize tentacle-specific cell types in a ctenophore. *Mol. Biol. Evol.* (2018).
538 doi:10.1093/molbev/msy171

539 36. De Graeve, F. *et al.* Identification of the *Drosophila* progenitor of mammalian Krüppel-like
540 factors 6 and 7 and a determinant of fly development. *Gene* **314,** 55–62 (2003).

541 37. Weber, U., Rodriguez, E., Martignetti, J. & Mlodzik, M. Luna, a Drosophila KLF6/KLF7,
542 is maternally required for synchronized nuclear and centrosome cycles in the preblastoderm
543 embryo. *PLoS One* **9,** e96933 (2014).

544 38. Blakeley, P. *et al.* Defining the three cell lineages of the human blastocyst by single-cell
545 RNA-seq. *Development* **142,** 3613 (2015).
546 39. Horridge, G. A. Presumed photoreceptive cilia in a ctenophore. *Quart J Micr Sci* **105,** 311–
547 317 (1964).
548 40. Schnitzler, C. E. *et al.* Genomic organization, evolution, and expression of photoprotein and
549 opsin genes in *Mnemiopsis leidyi*: a new view of ctenophore photocytes. *BMC Biol.* **10,** 107
550 (2012).
551 41. Ilsley, M. D. *et al.* Krüppel-like factors compete for promoters and enhancers to fine-tune
552 transcription. *Nucleic Acids Res.* **45,** 6572–6588 (2017).
553 42. Aksoy, I. *et al.* Klf4 and Klf5 differentially inhibit mesoderm and endoderm differentiation
554 in embryonic stem cells. *Nat. Commun.* **5,** 3719 (2014).
555 43. Tamm, S. L. Patterns of comb row development in young and adult stages of the
556 ctenophores *Mnemiopsis leidyi* and *Pleurobrachia pileus*. *J. Morphol.* **273,** 1050–1063
557 (2012).
558 44. Sebé-Pedrós, A. *et al.* Early metazoan cell type diversity and the evolution of multicellular
559 gene regulation. *Nat Ecol Evol* **2,** 1176–1188 (2018).
560 45. Harbison, G. R. & Miller, R. L. Not all ctenophores are hermaphrodites. Studies on the
561 systematics, distribution, sexuality and development of two species of *Ocyropsis*. *Mar. Biol.*
562 **90,** 413–424 (1986).
563 46. Pang, K. & Martindale, M. Q. Ctenophore whole-mount in situ hybridization. *CSH Protoc.*
564 **2008,** db.prot5087 (2008).
565 47. Schindelin, J. *et al.* Fiji: an open-source platform for biological-image analysis. *Nature*
566 *Methods* **9,** 676–682 (2012).

567 48. Kistler, K. E., Vosshall, L. B. & Matthews, B. J. Genome engineering with CRISPR-Cas9
568 in the mosquito Aedes aegypti. *Cell Rep.* **11,** 51–60 (2015).
569 49. Varshney, G. K. *et al.* High-throughput gene targeting and phenotyping in zebrafish using
570 CRISPR/Cas9. *Genome Res.* **25,** 1030–1042 (2015).
571 50. Xiao, A. *et al.* CasOT: a genome-wide Cas9/gRNA off-target searching tool. *Bioinformatics*
572 **30,** 1180–1182 (2014).
573 51. Moreland, R. T. *et al.* A customized Web portal for the genome of the ctenophore
574 *Mnemiopsis leidyi*. *BMC Genomics* **15,** 316 (2014).

575

576 **ACKNOWLEDGEMENTS**

577 This work was supported in part by startup funds from the University of Miami College of Arts
578 and Sciences to WEB. JSP was supported by the University of Miami College of Arts and
579 Sciences. We thank Ricardo Cepeda for additional animal support.

580

581 **AUTHOR CONTRIBUTIONS**

582 WEB originally conceived the study and designed the research. JSP and WEB performed
583 experiments, collected and analyzed data, and wrote the manuscript. JSP and WEB read and
584 approved the final manuscript.

585

586 **AUTHOR INFORMATION**

587 Correspondence and requests for materials should be addressed to WEB.
588 (w.browne@miami.edu)

589

590 **Competing financial interests:** The authors declare no competing financial interests.

Table1

Table 1 | Primers and Oligonucleotides used in this study. All sequences are oriented 5'-3'. Blue nucleotide sequences correspond to T7 promoter. Black bold italicized nucleotide sequences correspond to genomic *MleKlf* targets and include addition of two 5' *G* residues to aid T7 polymerase binding. Red nucleotide sequences denote region of complementary between templated primers and Universal tracrRNA primer, which are annealed to the form the sgRNA transcription template.

Name	Use	Forward	Reverse
MleKlf5a	ISH probe	ATGAGTGCTATGACATG	AAACGTGTTCAAATGCCTCTT
MleKlf5b	ISH probe	ATGGACGTTTCCACGC	AGACGAGCTAGGGGGAACG
MleKlfX	ISH probe	GGCAGTTTAGTTCGATCGG	TGCAGTGAGTGGTAGGTT
MleKlf5a sbMO#1	sbMO	TCTCGTGTCTGAAACAATTTTAAGT	n/a
MleKlf5a sbMO#2	sbMO	GTCTACCACCTGCAAGATTTTAAGT	n/a
MleKlf5b sbMO#1	sbMO	CAGTTGATTTCTCACCTGCCAAGAA	n/a
MleKlf5b sbMO#2	sbMO	CAAACAGACTTACCTTCAAATGTGA	n/a
Standard Control	sbMO	CCTCTTACCTCAGTTACAATTTATA	n/a
MleKlf5a sbMO RT-PCR	sbMO validation	CCCTTGTAAACTTGAGCA	TCTTCGTGTAAACCTTCG
MleKlf5b sbMO RT-PCR	sbMO validation	GACAAGTTCCAAAGACTAAC	TACAGTAGATGAGGAGGTTT
Universal tracrRNA	sgRNA synthesis	AAAAGCACCGACTCGGTGCCACTTTTTCAAGTTGATAACGGACTAGCCTTATTTTAACTTGCTATTTCTAGCTCTAAAAC	n/a
sgRNA template	sgRNA synthesis	GAAATTAATACGACTCACTATA**GG[N_{XX}]**GTTTTAGAGCTAGAAATAGC	n/a
MleKlf5a-gRNA1	sgRNA synthesis	AGCAACGGGTCCGTCCGT	n/a

Table1

MleKlf5a-gRNA2	sgRNA synthesis	TTGAGGGACGCGGGAGCAA	n/a
MleKlf5a-gRNA3	sgRNA synthesis	ACGGAGGGAATCGGCGAT	n/a
MleKlf5a-gRNA4	sgRNA synthesis	TTAGACTCTGTCGCGGGG	n/a
MleKlf5b-gRNA1	sgRNA synthesis	TGGTGATATACCAGGCG	n/a
MleKlf5b-gRNA2	sgRNA synthesis	ATCTTTCACGCTTAGGGGC	n/a
MleKlf5b-gRNA3	sgRNA synthesis	CGCTTGGAGGGAACCTAA	n/a
MleKlf5b-gRNA4	sgRNA synthesis	CTGAAACACCGGTCGCAG	n/a
MleKlf5a-sgRNA4 sequencing	sgRNA/Cas9 cut site validation	AAGACGTCCGATATTCTCTC	GGTGATCACTCCTACTGAAA
MleKlf5b-sgRNA3 sequencing	sgRNA/Cas9 cut site validation	GGTGTTCATACCTAGACGAT	TGTGTCTGTGTATAGTCGAG

Table 2 | Off-target CRISPR/Cas9 loci with mismatches to either *MleKlf5a* or *MleKl5b* target sequence and primers used for Sanger sequencing. All sequences are oriented 5'-3'.

Locus ID	# Mismatches	Forward	Reverse
ML090223a	4 (*MleKlf5a-sgRNA4)*	AAATTGTTTGTGTTCACACT	AGTTTTCTTTGTTTTCAGGG
ML021138a	5 (*MleKlf5a-sgRNA4)*	CAGCTTCATTGTAAAGAGTC	TTAGTTCTTATGTTTTCGCG
ML200217a	5 (*MleKlf5b-sgRNA3)*	GGATACTAGTTCCATAGCAG	CTCCTTGTTGATATTCTGGA
ML00363a	6 (*MleKlf5b-sgRNA3)*	TATGATTCTTGTTACCAGGG	ACATACGTCATCCTATTAGC
ML02979a	7 (*MleKlf5b-sgRNA3)*	CTGCATGATTACAAAGGTTT	ATGCTAAGAAGGATGCAATA

Figure1

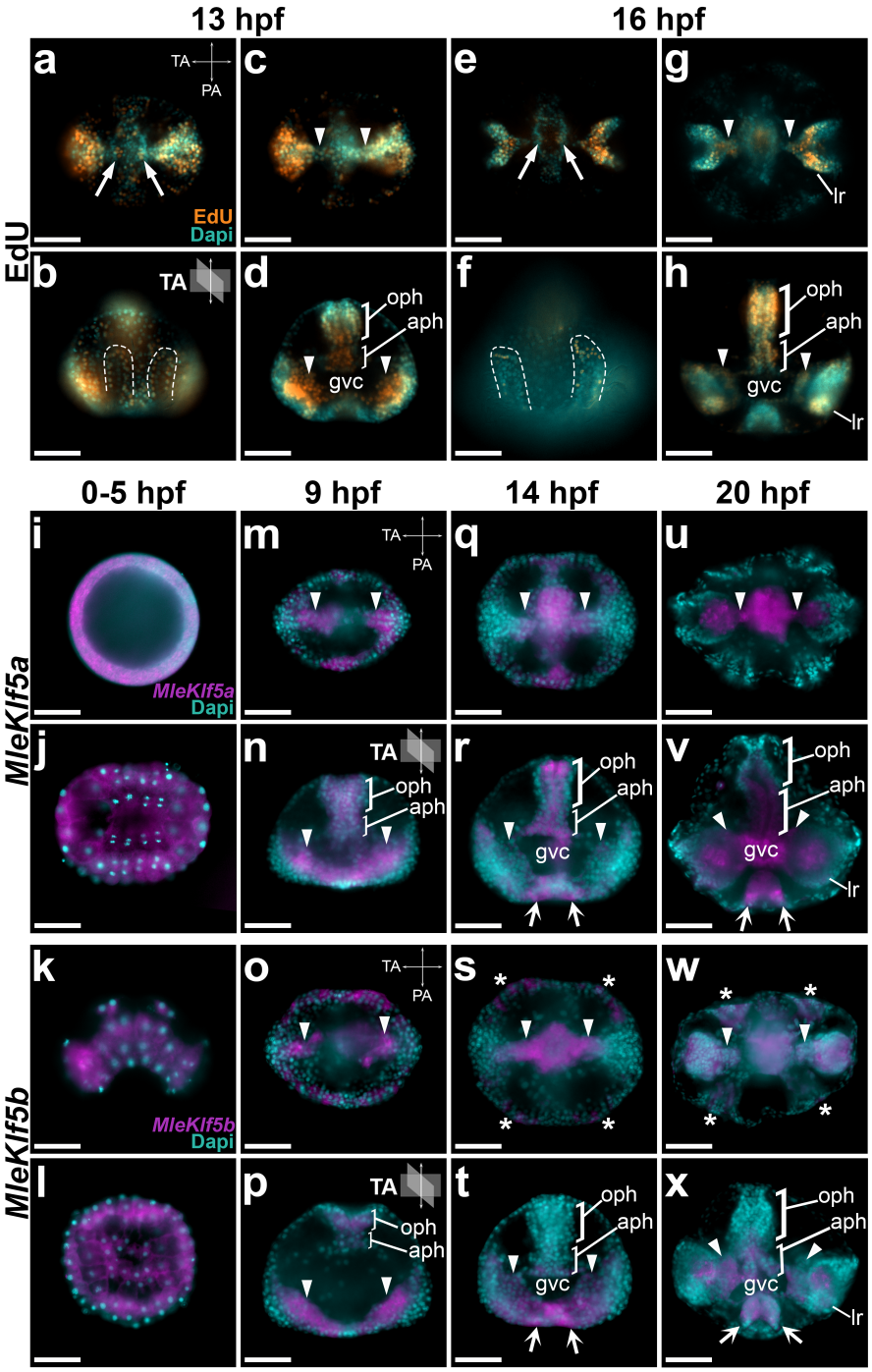

Figure 1. *MleKlf5a* and *MleKlf5b* are expressed in regions of rapid cell proliferation during embryogenesis in *Mnemiopsis leidyi.* Schematic depiction of tentacular axis (TA) and pharyngeal axis (PA) orientation are located in panel upper right. Aboral view in **a, c, e, g, j, l, m, o, q, s, u, w**. Lateral view, oral up, in **b, d, f, h, k, n, p, r, t, v, x**. Scale bars are 50 µm. **(a-h)** 25 min EdU pulse in 13 hours post fertilization (hpf) (**a-d**) and 16 hpf (**e-h**) embryos. EdU incorporation is localized to two cell clusters in the apical organ (**a, e**), epithelial cells flanking the developing ctene rows (bounded by dashed lines) (**b, f**), epithelial cells lining the gastrovascular cavity (gvc) (**d, h**) in the developing tentacular median ridges (arrowheads), and the oral (oph) and aboral (aph) regions of the pharynx (**d**). (**g, h**) Later in development, EdU incorporation is found in the tentacular median ridge (arrowheads) and lateral ridges (lr) of the tentacle bulbs and in both oral (oph) and aboral (aph) regions of the pharynx. (**i-x**) mRNA expression patterns for *MleKlf5a* and *MleKlf5b* during embryogenesis. Maternal transcripts for both *MleKlf5a* (**i, j**) and *MleKlf5b* (**k, l**) are found ubiquitously in zygotes (**i**), early cleavage stages (**k**) and gastrulae (**j, l**). (**m-p**) Zygotic *MleKlf5a* and *MleKlf5b* transcripts exhibit overlapping endodermal expression domains. At 9 hpf expression of *MleKlf5a* and *MleKlf5b* transcripts are localized to the forming tentacular median ridges (arrowheads) and the developing pharynx (oph + aph). (**q-t**) At 14 hpf *MleKlf5a* and *MleKlf5b* transcript expression is also found in the apical organ (arrows) and epithelia of the newly formed gastrovascular cavity (gvc). (**u-x**) At 20 hpf *MleKlf5a* and *MleKlf5b* transcripts are found in the tentacular median ridge (arrowheads) and lateral ridge (lr), on either side of the apical organ floor (arrows), localized towards the aboral end of the pharynx (aph), and the gastrovascular cavity epithelium (gvc).

Figure2

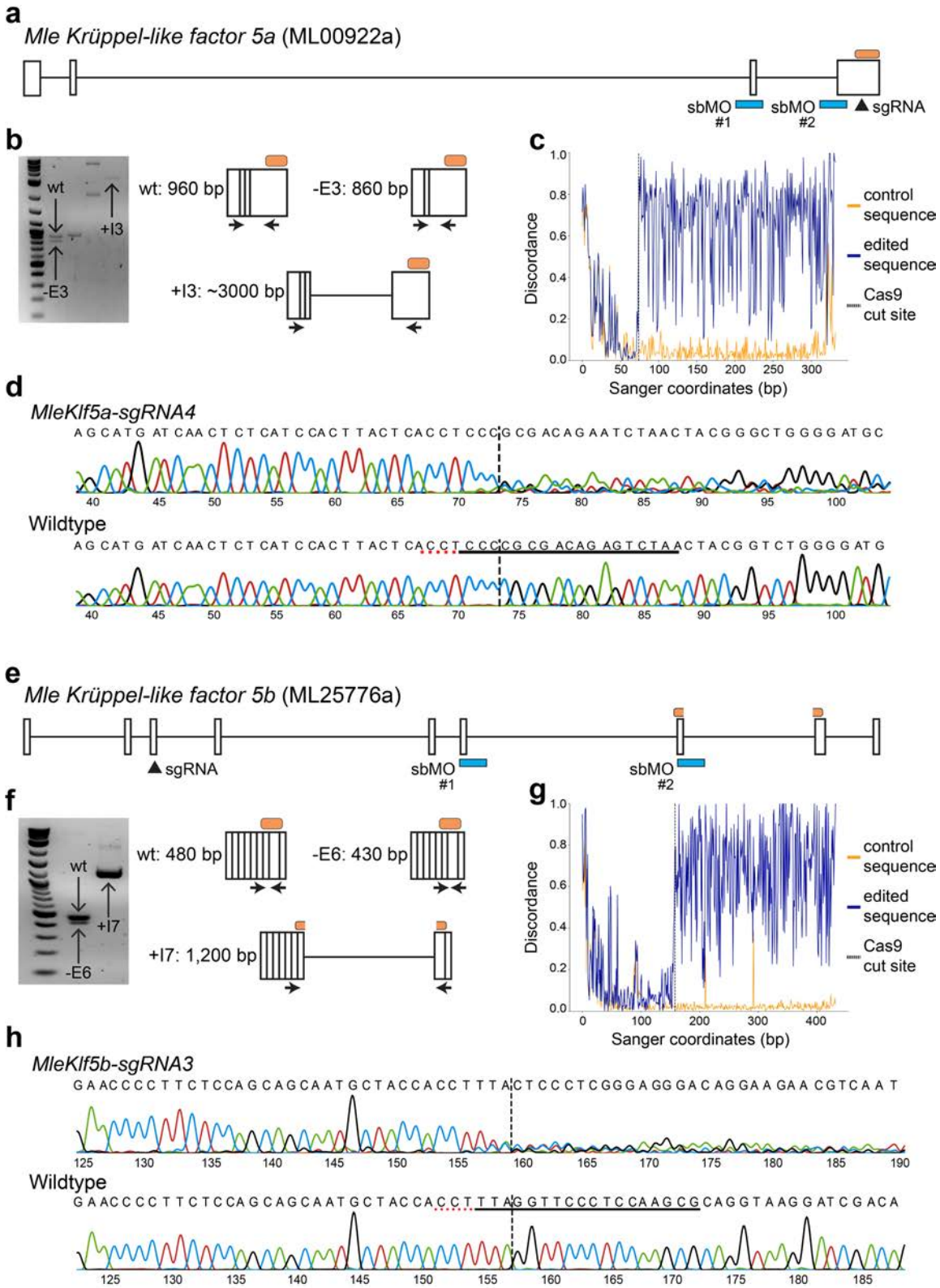

Figure 2. Two independent methods used to abrogate *MleKlf5a* and *MleKlf5b* gene function. *MleKlf5a* (**a**) and *MleKlf5b* (**e**) exon-intron schematics show the location of sbMO targets (blue boxes) and sgRNA targets (black triangle) used in this study. (**b,f**) Electrophoretic gels of PCR products obtained using *MleKlf5a* and *MleKlf5b* sbMO RT-PCR primers (arrows in predicted spliceform schematics to the right) on cDNA obtained from an individual morphant exemplar (n = 21 morphants), 2-log DNA ladder was used for band size reference. Wildtype (wt) and mis-spliced transcripts due to exon-skipping (-E) and/or intron retention (+I) were present in morphants. (**c-d, g-h**) Crispant discordance plots and corresponding Sanger sequence traces. sgRNA target site is underlined, Cas9 cut site is represented by dashed line and shows clearly elevated sequence discordance relative to genome sequence reference and control sanger sequencing. Sanger sequencing signal degradation is caused by the introduction of indels in an individual crispant exemplar (n = 17 crispants; also see **EDF3b**).

Fig3

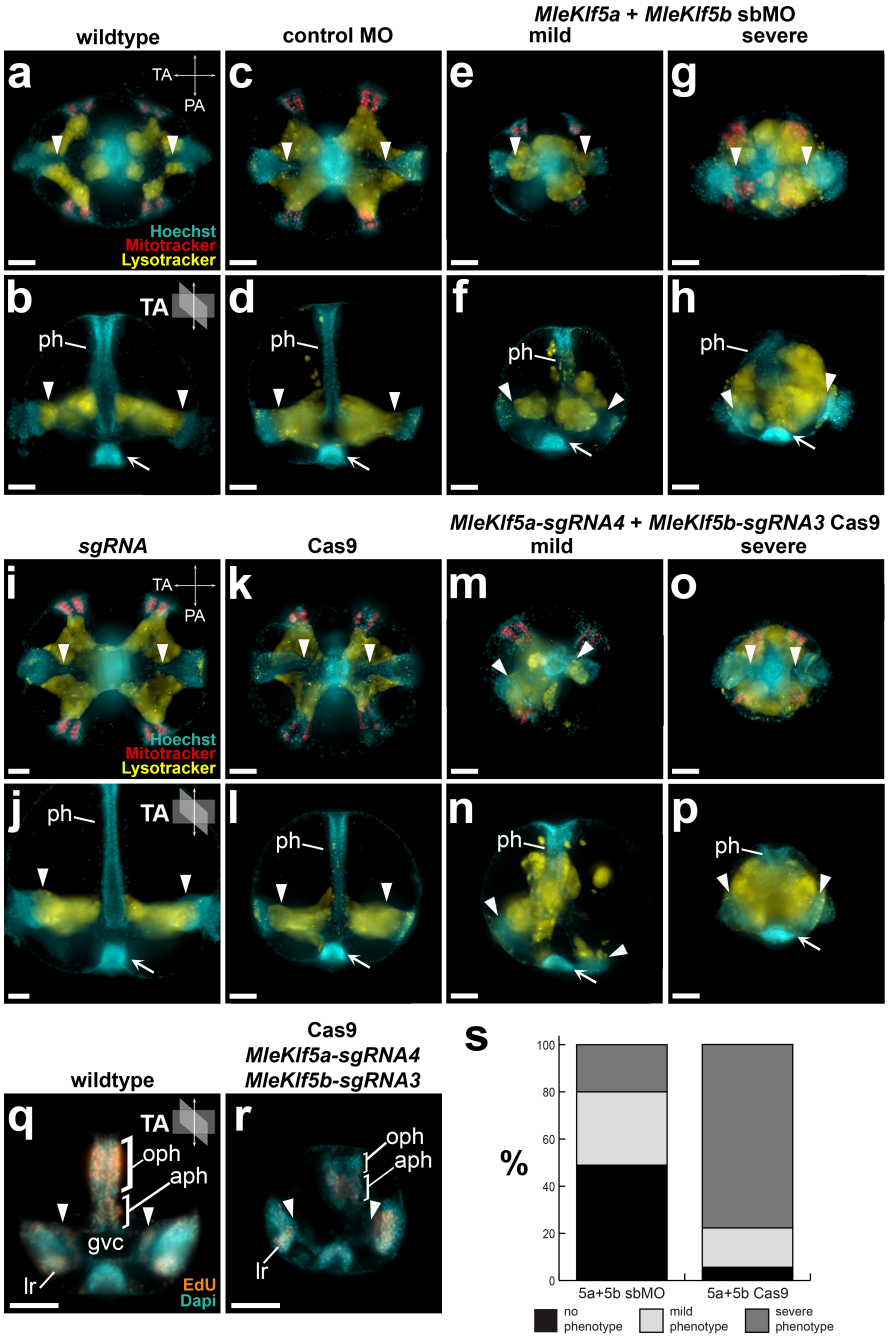

Figure 3. ***MleKlf5a* and *MleKlf5b* double gene knockdown via sbMO and *sgRNA*-Cas9 genome editing.** (**a-p**) Live imaging showing morphology of 20 hpf cydippids. Aboral view in **a, c, e, g, i, k, m, o**. Lateral view, oral up, in **b, d, f, h, j, l, n, p, q, r**. Schematic depiction of tentacular axis (TA) and pharyngeal axis (PA) orientation are located in panel upper right. Scale bars are 50 µm. Hoechst (blue) marks nuclei. Mitotracker (red) preferentially marks position of ctene row polster cells, one pair per embryonic quadrant. Lysotracker (yellow) preferentially stains epithelial cells lining the gastrovascular cavity (gvc). Tentacular median ridges (arrowheads) are positioned medially along the tentacular axis and contacted by gvc epithelial cells. The pharynx (ph) is positioned centrally and joins with the gvc aborally. The apical organ (arrow) is located at the aboral pole of the embryo. Un-injected wildtype embryo (**a, b**). Morphology is unaffected in embryos sham injected with control morpholino (MO) (**c, d**), *sgRNA* only (**i, j**) or Cas9 protein only (**k, l**). In contrast, mild phenotypes in double gene knockdown morphants (**e, f**) and double gene edited crispants (**m, n**) display aberrant distributions of gvc epithelial cells (Lysotracker signal), aberrant patterning of the pharynx (ph) including aboral bifurcations (**f**, **n**, **EDF4**, **EDF5**), aberrant patterning of the tentacle bulb and tentacular median ridges (arrowheads), and atypical apical organ (arrow) morphology. Severe phenotypes in double gene knockdown morphants (**g, h**) and double gene edited crispants (**o, p**) are reduced in size due to lack of mesogleal ECM extrusion, display collapsed pharynx with gvc junction defects, significantly reduced tentacle bulbs and tentacular median ridges (arrowheads), and apical organ defects (arrow). (**q**) 25 min EdU pulse in wildtype 16 hpf embryo. Strong EdU incorporation signal (orange) is found in the oral (oph) and aboral (aph) regions of the developing pharynx, epithelial cells lining the gastrovascular cavity (gvc), the developing tentacular median ridges (arrowheads) and lateral ridges (lr) of the tentacle bulbs. (**r**) 25 min EdU pulse in 16 hpf crispant embryo. EdU incorporation signal (orange) is significantly diminished in regions that also express *MleKlf5a* and *MleKlf5b* (refer to **Fig. 1**) including the pharynx, gvc and tentacular median ridges. Note that lr cell proliferation is not affected. (**s**) Comparison of phenotypic proportions in morphants ($n = 45$) (51% no phenotype, 29% mild phenotype, 20% severe phenotype) vs crispants ($n = 16$) (6% no phenotype, 19% mild phenotype, 75% severe phenotype).

Fig4

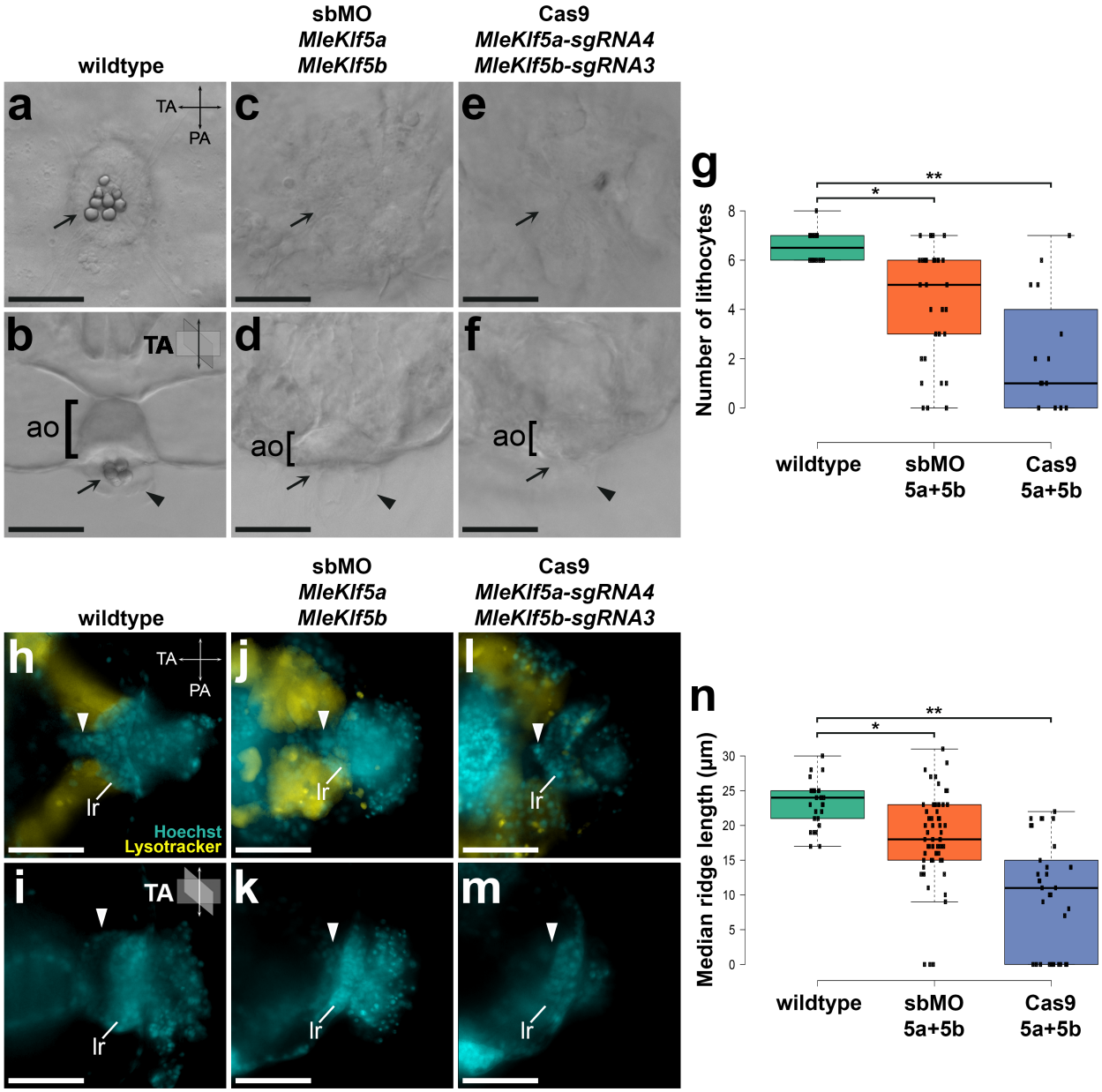

Figure 4. *MleKlf5a* and *MleKlf5b* double gene knockdown negatively affects apical organ lithocyte production and negatively affects tentacular median ridge size. Live images of embryos at 20 hpf. Schematic depiction of tentacular axis (TA) and pharyngeal axis (PA) orientation are located in panel upper right. Aboral view in **a, c, e, h, j, l**. Lateral view, oral up, in **b, d, f, i, k, m**. Scale bars are 50 µm. (**a, b**) lithocytes (arrow), dome cilia (arrowhead) and apical organ (ao) in wildtype embryo. (**c, d**) double gene knockdown morphant lacking lithocytes. (**e, f**) double gene edited crispant lacking lithocytes. Dome cilia (arrowheads) and balancer cilia are present in both morphants and crispants. (**g**) *MleKlf5a* and *MleKlf5b* double gene knockdown significantly reduces lithocyte production. Box plot center lines show medians, box limit at 25th and 75th percentiles, whiskers extend 1.5 times interquartile range from the 25th and 75th percentiles, data points are plotted as open circles. * = two-tailed *t*-test, = 3.47, <0.005. ** = two-tailed *t*-test, = 6.52, <0.00001. Wildtype (n = 14), morphant (n = 33), crispant (n = 15). (**h, i**) Wildtype tentacular median ridge (arrowhead) and lateral ridge (lr). (**j, k**) double gene knockdown morphant with dramatically reduced tentacular median ridge. (**l, m**) double gene edited crispant with dramatically reduced tentacular median ridge. The tentacle bulb lateral ridge remains present in both morphants and crispants. (**n**) *MleKlf5a* and *MleKlf5b* double gene knockdown significantly reduces tentacular median ridge length. Box plot center lines show the median, box limit at 25th and 75th percentiles, whiskers extend 1.5 times interquartile range from the 25th and 75th percentiles, data points are plotted as open circles. * = two-tailed *t*-test, = 4.01, <0.0005. ** = two-tailed *t*-test, = 8.32, <0.00001. Each data point represents a single tentacular median ridge length, with a maximum of 2 data points (i.e., 2 tentacular median ridges) from each embryo. Data value of 0 indicate the absence of a tentacular median ridge and/or tentacle bulb. Wildtype (n = 28), morphant (n = 61), crispant (n = 34).

EDF1

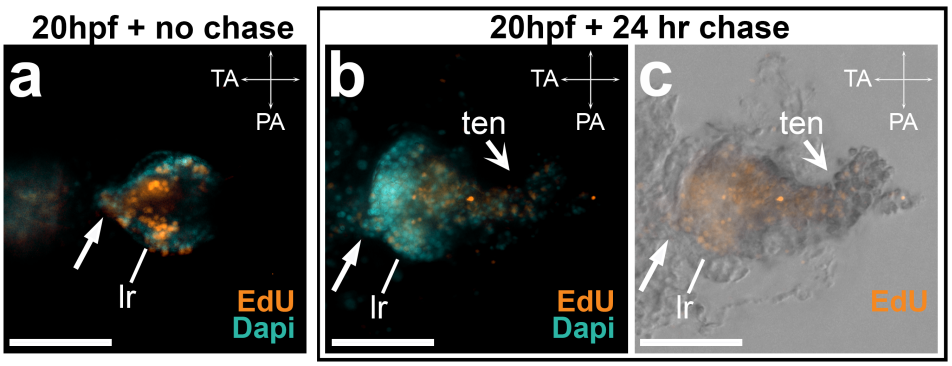

Extended Data Figure 1. Proliferating cells in the tentacular median ridge give rise to tentacle muscle in *M. leidyi*. Aboral view and schematic depiction of tentacular axis (TA) and pharyngeal axis (PA) orientation are located in panel upper right. Scale bars are 50 µm. EdU pulse:chase immunohistochemistry on tentacle bulbs (**a**) after 25 min pulse:0 min chase and (**b**) after 25 min pulse:24 hr chase. (**a**) 25 min pulse EdU marks rapidly proliferating cells in the tentacular median ridge (arrow) and lateral ridges (lr) of the tentacle bulb. (**b**) After 25 min pulse:24 hr chase, EdU incorporation is primarily detected in emergent tentacle muscle cells.

EDF2

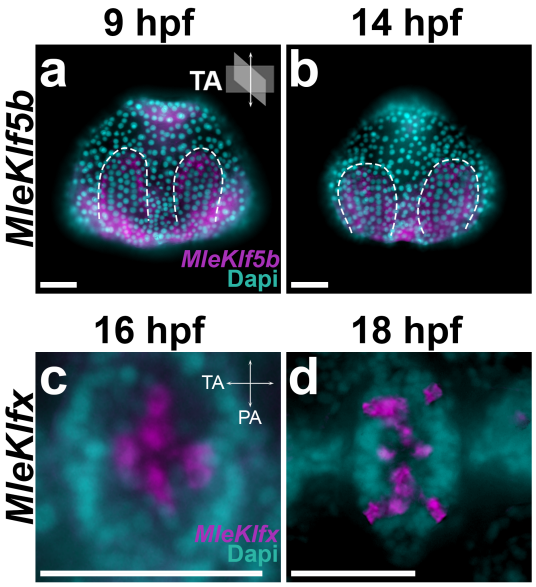

Extended Data Figure 2. Additional *MleKlf5b* and *MleKlfX* transcript expression domains. Schematic depiction of tentacular axis (TA) and pharyngeal axis (PA) orientation are located in panel upper right. Scale bars are 50 µm. (**a, b**) 9 hpf and 14 hpf embryos, lateral view, oral up. Dashed lines bound *MleKlf5b* ectodermal expression (magenta) in rapidly dividing cells (compare with **Fig. 1b, f**) that flank developing ctene row pairs (visible as aligned columns of DAPI stained nuclei bounded by *MleKlf5b* expression). (**c, d**) Magnified aboral views of *MleKlfX* expression (magenta) in epithelial floor cells of the apical organ. (**c**) Initially *MleKlfX* expression is detected at 16 hpf in four small clusters of cells at the boundary of each developing embryonic quadrant converging in the center of the apical organ. (**d**) Expression of *MleKlfX* resolves into several cell clusters by 18 hpf in both the tentacular (TA) and pharyngeal (PA) axes.

EDF3

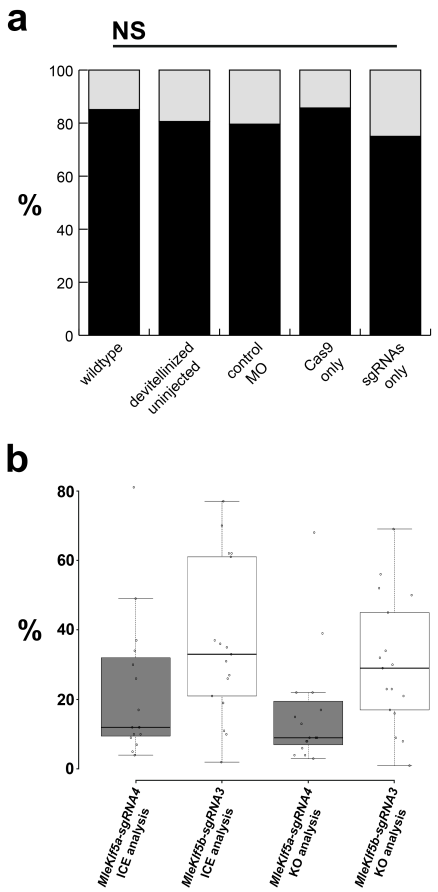

Extended Data Figure 3. ICE analysis of Crispants. (**a**) Sham injection has no effect on embryonic development. Bar graph comparison of percentage of normal development in wildtype $n = 161$ (24 abnormal); devitellinized but uninjected $n = 217$ (42 abnormal), two-tailed Fisher's exact test P=0.2761; control MO injected $n = 49$ (10 abnormal), two-tailed Fisher's exact test P=0.379; Cas9 only injected $n = 7$ (1 abnormal), two-tailed Fisher's exact test P=1; sgRNA only injected $n = 4$ (1 abnormal), two-tailed Fisher's exact test P=0.4851. (**b**) Distribution of ICE scores (estimate of indel proportion in signal trace from genomic DNA of individual crispants) and KO scores (estimate of indel proportion that result in frameshift mutation) for *MleKlf5a-sgRNA4* ($n = 14$) and *MleKlf5b-sgRNA3* ($n = 17$). Cas9 cut sites were PCR amplified from genomic DNA prepared from individual crispants and subsequently Sanger sequenced. Each cut site data point represents Sanger trace analyses from an individual embryo. Box plot center lines show the median, box limit at 25th and 75th percentiles, whiskers extend 1.5 times interquartile range from the 25th and 75th percentiles, data points are plotted as open circles.

EDF4

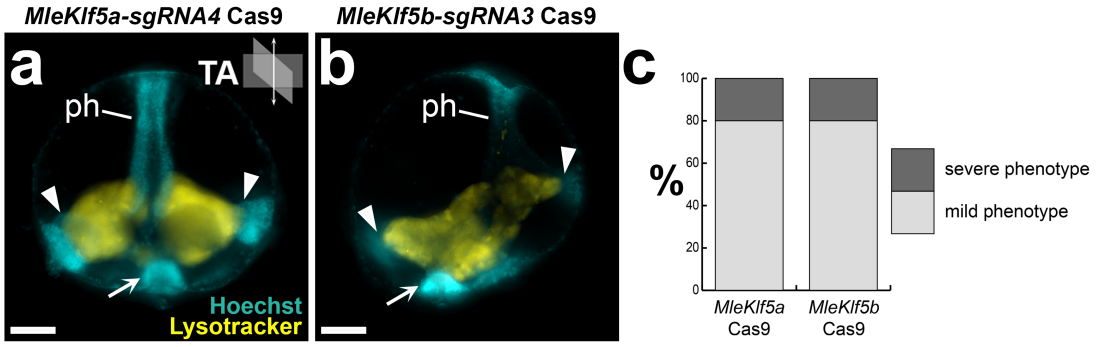

Extended Data Figure 4. Cas9 mediated genome editing of either *MleKlf5a* or *MleKlf5b* resulted in reduced phenotype penetrance. Schematic depiction of tentacular axis (TA) orientation located in panel upper right. Lateral view, oral up, scale bars are 50 µm. Single gene editing produced primarily mild phenotypes for both *MleKlf5a* crispants (**a**) and *MleKlf5b* crispants (**b**). (**c**) Bar graph comparison of distribution of mild (gray) vs severe (black) phenotypes in *MleKlf5a* crispants ($n = 5$, 80% mild) and *MleKlf5b* crispants ($n = 5$, 80% mild).

EDF5

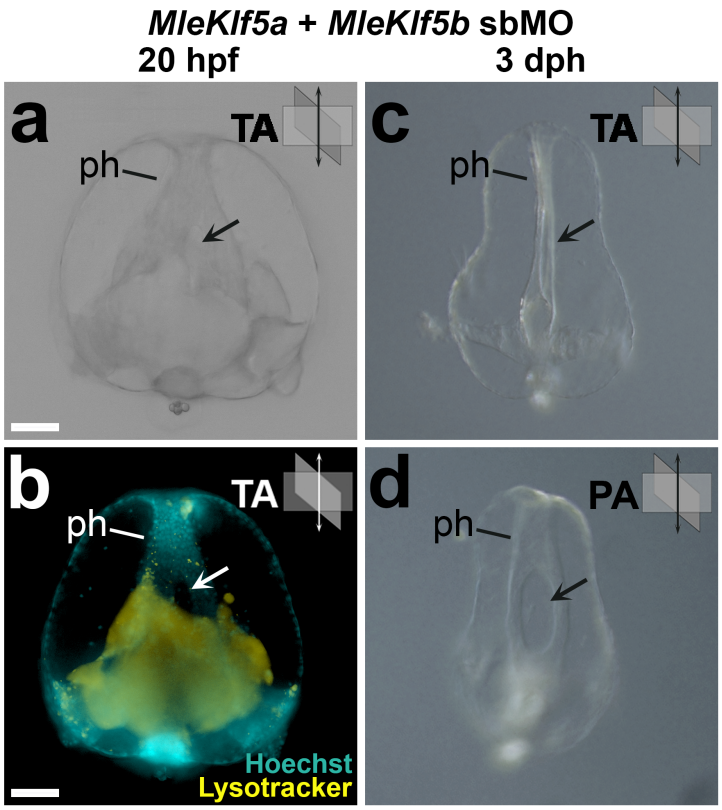

Extended Data Figure 5. Aberrant pharyngeal patterning. Schematic depiction of tentacular axis (TA) and pharyngeal axis (PA) orientation located in panel upper right. Lateral views, oral up, scale bars are 50 µm. (**a, b**) 20 hpf double gene morphant embryo with bifurcated (arrow) pharynx (ph). (**c, d**) Same individual morphant 3 days post fertilization (dph) showing persistence of pharyngeal bifurcation patterning defect just anterior of the pharyngeal-gastrovascular junction resulting in a deletion of the pharyngeal folds.

EDF6

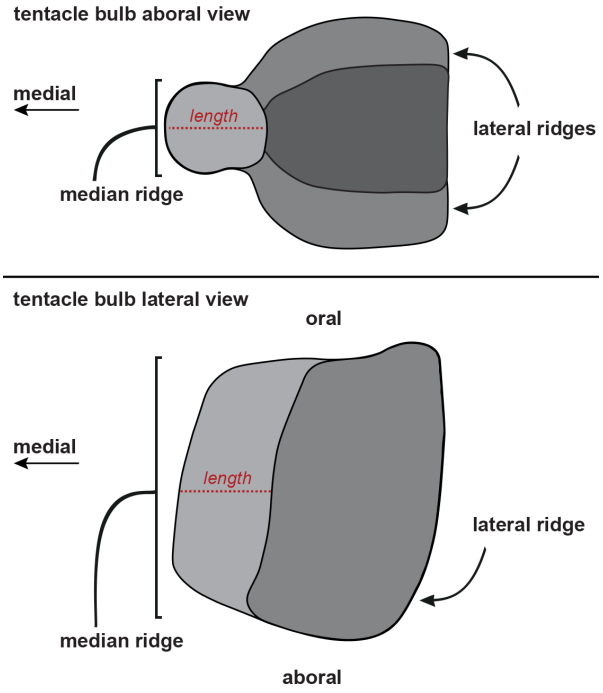

Extended Data Figure 6. Cydippid tentacle bulb schematic. Aboral top, lateral bottom. Tentacular median ridge colored light gray. Tentacular lateral ridges colored darker gray. Tentacle (not shown) is rooted at the aboral medial base of the tentacle bulb. Location of measurement taken for the tentacular median ridge length (refer to **Fig. 4n**) is denoted with red dashed line.